University of Reading

The onset and cessation of seasonal rainfall over Africa

Article

Published Version

Creative Commons: Attribution 4.0 (CC-BY)

Open Access

Dunning, C. M. ORCID: https://orcid.org/0000-0002-7311-7846, Black, E. C. L. ORCID: https://orcid.org/0000-0003-1344-6186 and Allan, R. P. ORCID: https://orcid.org/0000-0003-0264-9447 (2016) The onset and cessation of seasonal rainfall over Africa. Journal of Geophysical Research: Atmospheres, 121 (19). pp. 11405-11424. ISSN 2169-8996 doi: 10.1002/2016JD025428 Available at https://centaur.reading.ac.uk/66825/

It is advisable to refer to the publisher's version if you intend to cite from the work. See Guidance on citing.
Published version at: http://dx.doi.org/10.1002/2016JD025428
To link to this article DOI: http://dx.doi.org/10.1002/2016JD025428

Publisher: American Geophysical Union

All outputs in CentAUR are protected by Intellectual Property Rights law, including copyright law. Copyright and IPR is retained by the creators or other copyright holders. Terms and conditions for use of this material are defined in the End User Agreement.

www.reading.ac.uk/centaur

University of Reading

CentAUR

Central Archive at the University of Reading

Reading's research outputs online

AGU PUBLICATIONS

JGR

Journal of Geophysical Research: Atmospheres

RESEARCH ARTICLE

10.1002/2016JD025428

Key Points:
- Diagnosed patterns in onset/cessation of African rainy seasons, produced using an adapted method, are compatible with physical drivers
- Consistent onset/cessation characteristics in satellite-based rainfall data, ERA-Interim deficient for biannual regime
- Rainy season cessation over the Horn of Africa is 7 days later in El Nino years and 5 days earlier in La Nina

Supporting Information:
- Supporting Information S1

Correspondence to:
C. M. Dunning,
c.m.dunning@pgr.reading.ac.uk

Citation:
Dunning, C. M., E. C. L. Black, and R. P. Allan (2016), The onset and cessation of seasonal rainfall over Africa, *J. Geophys. Res. Atmos.*, *121*, 11,405–11,424, doi:10.1002/2016JD025428.

Received 30 MAY 2016
Accepted 14 SEP 2016
Accepted article online 17 SEP 2016
Published online 8 OCT 2016

©2016. The Authors.
This is an open access article under the terms of the Creative Commons Attribution License, which permits use, distribution and reproduction in any medium, provided the original work is properly cited.

The onset and cessation of seasonal rainfall over Africa

Caroline M. Dunning[1], Emily C. L. Black[1,2], and Richard P. Allan[1,2,3]

[1]Department of Meteorology, University of Reading, Reading, UK, [2]NCAS-Climate, University of Reading, Reading, UK, [3]National Centre for Earth Observation, UK

Abstract Variation in the seasonal cycle of African rainfall is of key importance for agriculture. Here an objective method of determining the timing of onset and cessation is, for the first time, extended to the whole of Africa. The method is applied to five observational data sets and the ERA-Interim reanalysis. Compatibility with known physical drivers of African rainfall, consistency with indigenous methods, and generally strong agreement between satellite-based rainfall data sets confirm that the method is capturing the correct seasonal progression of African rainfall. The biannual rainfall regime is correctly identified over the coastal region of Ghana and the Ivory Coast. However, the ERA-Interim reanalysis exhibits timing biases over areas with two rainy seasons, and both ERA-Interim and the ARCv2 observational data set exhibit some inconsistent deviations over West Africa. The method can be used to analyze both seasonal-interannual variability and long-term change. Over East Africa, we find that failure of the rains and subsequent humanitarian disaster is associated with shorter as well as weaker rainy seasons, e.g., on average the long rains were 11 days shorter in 2011. Cessation of the short rains over this region is 7 days later in El Niño and 5 days earlier in La Niña years with only a small change in onset date. The methodology described in this paper is applicable to multiple data sets and to large regions, including those that experience multiple rainy seasons. As such, it provides a means for investigating variability and change in the seasonal cycle over the whole of Africa.

1. Introduction

Much has been postulated on past changes in African rainfall, including changes in the timing of the seasonal cycle and shifts in the beginning and end of the wet seasons. Anecdotal evidence from farmers in the region of West Africa south of the Sahel suggests a forward shift in the onset of the rainy season [*Van de Giesen et al.*, 2010]. However, evidence of this type is not always indicative of meteorological changes [e.g., *Rao et al.*, 2011], and other studies of this region found no significant trend [*Sanogo et al.*, 2015]. Future changes in tropical circulation patterns may alter the seasonality and lead to increasing uncertainty in the timing of rainy seasons [*Feng et al.*, 2013]. For example, the northward extension of rainfall and increase in August rainfall in the Sahel [*Dong and Sutton*, 2015; *Sanogo et al.*, 2015] may be related to the reduction in August rainfall south of the Sahel [*Sanogo et al.*, 2015] and changes in the onset and duration of the "little dry season" that occurs along the West African coast during the summer months [*Okoloye et al.*, 2014].

In order to assess whether the seasonality is indeed undergoing large-scale shifts and to attribute potential drivers, a generally applicable method of identifying the onset and cessation of the wet season is required. Many previous studies examining the nature of the onset and cessation of rainfall have been conducted, but for the most part, these have focused on the national to regional scale [*Liebmann et al.*, 2012]. Relating changes and variability in seasonality to wider-scale drivers and physical mechanisms demands a method for determining onset that is applicable across the entirety of continental Africa that experiences a wet season, including those regions with two seasons per year. The method must robustly capture the seasonal cycle across Africa in an automated manner across multiple data sets in order to be applicable to the evaluation and interpretation of climate model simulations.

We present a new method for determining onset and cessation in regions, such as the Horn of Africa that experience two wet seasons per year [*Lyon and DeWitt*, 2012]. This, combined with the onset method of *Liebmann and Marengo* [2001] and *Liebmann et al.* [2012], allows onset and cessation dates to be objectively derived for the whole of Africa. The recent publication of daily precipitation data sets for Africa for periods longer than 30 years allows for analysis of variability, which was not possible in the study of *Liebmann et al.* [2012] due to the short records. This is especially relevant in the context of recently described discrepancies

between observed African rainfall data sets, including rainfall underestimation over West Africa [*Maidment et al.*, 2015, 2014; *Tarnavsky et al.*, 2014], and the effect of observational coverage on perceived long-term change in tropical rainfall [*Balan Sarojini et al.*, 2012]. Understanding variability and change is essential for interpreting recent changes in African rainfall [*Lyon and DeWitt*, 2012; *Lott et al.*, 2013]. Assessing whether data sets which exhibit different rainfall biases are consistent in seasonality offers greater understanding of different precipitation data sets and their relative strengths [*Awange et al.*, 2016]. The relative paucity of gauge based data over Africa often results in the use of reanalysis rainfall data [*Fitzpatrick et al.*, 2015; *Mounkaila et al.*, 2015; *Shongwe et al.*, 2015; *Yang et al.*, 2015a], which is compared here alongside satellite-based precipitation estimates.

The remainder of the paper is structured as follows: in section 2 the method and its implementation are described. Section 3 compares the seasons identified first to those expected from the published literature on the dynamical drivers of African rainfall and second to agriculturally defined seasons. Section 4 demonstrates the applicability of this definition of seasonality to six data sets. Section 5 gives an example of how this method can be used to explore variability. Section 6 contains the discussion and conclusions.

2. Methodology and Data Sets

2.1. Data Sets

For this study we require multiple precipitation data sets, at daily resolution, for the entirety of continental Africa. In order to assess whether the method is applicable across data sets with varying rainfall amounts and intensity we have chosen data sets to encompass a range of methodologies of rainfall estimation. Only those that are available for a sufficient period to analyze variability (at least 15 years) were considered. Due to the limited availability of daily rain gauge data (see http://www.ecmwf.int/en/forecasts/charts/monitoring/dcover), five gridded combined satellite/gauge-based estimates and one reanalysis product are used. The data sets and main characteristics are summarized in Table 1.

African Rainfall Climatology version 2 (ARCv2) is a daily precipitation estimation data set produced by the National Oceanic and Atmospheric Administration (NOAA)/National Centers for Environmental Prediction/Climate Prediction Centre (CPC) for use in famine early warning systems [*Novella and Thiaw*, 2013]. ARCv2 uses infrared data, from the 3-hourly geostationary EUMETSAT (European Organization for the Exploitation of Meteorological Satellites), and gauge observations from the Global Telecommunication System. In addition to thermal infrared (TIR) and rain gauge data, the Global Precipitation Climatology Project (GPCP) data set also uses passive microwave [*Huffman et al.*, 2001]. This data set, however, is available at lower resolution (1° compared to 0.1°) and is only available from 1997 at daily resolution, whereas ARCv2 extends back to 1983. Similarly, the Tropical Rainfall Measuring Mission (TRMM) Multisatellite Precipitation Analysis is also only available from 1998. Here we have used the 3B42 research derived daily product, formed of 3-hourly combined microwave-infrared (IR) estimates (with gauge adjustment) and monthly combined microwave-IR-gauge estimates of precipitation [*Huffman et al.*, 2007].

The Climate Hazards Group InfraRed Precipitation with Stations (CHIRPS) data set also uses TIR imagery and gauge data in addition to a monthly precipitation climatology, CHPClim, and atmospheric model rainfall fields from the NOAA Climate Forecast System, version 2 (CFSv2) [*Funk et al.*, 2015]. Despite CHIRPS being available at higher resolution (0.05° compared with 0.25°), CHIRPS also includes TRMM 3B42; therefore, we expect to find similarities between these data sets after 1998, when TRMM becomes available, whereas CHIRPS extends back to 1983. CHIRPS is the only data set used which includes a monthly climatology.

In common with previous data sets, the TAMSAT (Tropical Applications of Meteorology using SATellite data and ground-based observations) African Rainfall Climatology and Time series (TARCATv2) data set uses TIR to give precipitation estimates; however, unlike the previous data sets, gauge observations are used only for the spatially varying time invariant calibration, whereas the other data sets, such as ARCv2, merge in contemporaneous gauge data [*Maidment et al.*, 2014; *Tarnavsky et al.*, 2014].

ERA-Interim (ERA-I) reanalysis simulated precipitation was also used. ERA-I is a reanalysis of the global atmosphere produced using the European Centre for Medium Range Weather Forecasts' (ECMWF) Integrated Forecast System combined with data assimilation [*Dee et al.*, 2011]. Here 12-hourly total precipitation on a 0.75° grid was used.

Table 1. Description of Some of the Characteristics of the Data Sets of African Precipitation Used in This Study[a]

Data	Inputs	Spatial Resolution	Period Used	Reference
TARCATv2	TIR	0.0375°	1984–2014	*Maidment et al.* [2014]
ARCv2	IR, gauges	0.1°	1983–2013	*Novella and Thiaw* [2013]
GPCP 1DD	TIR, PMW, gauges	1°	1997–2014	*Huffman et al.* [2001]
TRMM 3B42	TIR, VIS, PMW, radar, gauges	0.25°	1998–2014	*Huffman et al.* [2007]
CHIRPS	CHPClim, TIR, TRMM 3B42, CFSv2, gauges	0.05°	1981–2014	*Funk et al.* [2015]
ERA-Interim	ECMWF Forecast System	0.75°	1983–2014	*Dee et al.* [2011]

[a]TIR, Thermal InfraRed Imagery; IR, InfraRed Imagery; PMW, passive microwave; VIS, visible; CHPClim, monthly precipitation climatology; and CFSv2, atmospheric model rainfall fields from the NOAA Climate Forecast System version 2.

For this analysis, all the data sets have been interpolated onto the GPCP 1DD grid and have a spatial resolution of 1°. All the observational data sets are at daily resolution, and ERA-I was converted from 12-hourly to daily resolution.

2.2. Extension of the Liebmann Method for All of Africa

In this study, the method used by *Liebmann et al.* [2012] to produce a precipitation climatology for the entire African continent was employed to identify the onset and cessation. This method has been used over Kenya and Tanzania for observational data sets [*Boyard-Micheau et al.*, 2013; *Camberlin et al.*, 2009] and to assess regional climate models over West Africa [*Diaconescu et al.*, 2015]. The method is described below in sections 2.2.1–2.2.3. Their method for finding onset was based on that of *Liebmann and Marengo* [2001] and has three stages. First, harmonic analysis applied to the whole time series for each grid point is used to determine if one or two wet seasons are experienced per year. The start and end of the period when the wet season usually occurs is then found; this is termed the "climatological water season." The onset and cessation in each individual year is then found. The onset and cessation dates are determined by finding the minima and maxima, respectively, in the cumulative daily precipitation anomaly, which increases when the daily precipitation is above the climatological mean daily rainfall, and decreases when the daily precipitation is below the climatological mean daily rainfall.

When considering the Horn of Africa, *Liebmann et al.* [2012] defined the broad seasons when the long and short rains are expected to occur, as their method did not determine the seasons when rainfall occurs for regions with two wet seasons per year. They did not examine the onset and cessation over other regions that experience two wet seasons a year, such as the West Africa southern coastal region (coast of Ghana and the Ivory Coast; region 4 in Figure 4). Thus, in this study, an alternative method is proposed for the first time to find the two periods when the wet seasons usually occur over such regions. The onset and cessation for each individual season is then found using the same method as that used for finding one season.

The following three subsections detail this application of *Liebmann et al.* [2012]'s method. First, harmonic analysis used to determine the number of seasons is described, followed by the method used for regions with one wet season per year, and finally, the new adaptation of *Liebmann et al.* [2012]'s method for two-season regions.

2.2.1. Categorizing the Seasonality

Harmonic analysis was used to define the number of wet seasons experienced per year. Here, we describe regions that experience one wet season per year as having an annual regime and regions that experience two wet seasons per year as having a biannual regime. For the small area in Ethiopia that experiences three wet seasons per year, only the two longest were considered, and it was classified as biannual. For each grid point, the amplitude of the first and second harmonics were computed. Figures 1a and 1b show the amplitude of the first and second harmonics, respectively, for the TARCATv2 data set. The ratio of the amplitude of the second harmonic to the amplitude of the first harmonic (Figure 1c) was used to determine the seasonality (similar results were found for all six data sets; Figure S1 in the supporting information). A ratio greater than 1.0 indicated a biannual point and a ratio less than 1.0 indicated a point with an annual regime. This contour is marked on Figure 1c as a dashed line. For locations which experience one short season with very low rainfall totals the second harmonic may fit the data better, thus giving a higher ratio even though there is just one wet season [*Liebmann et al.*, 2012]; therefore, results over regions such as the Sahara need to be carefully analyzed. The harmonic analysis approach is similar to that used in *Liebmann et al.* [2012] to determine the number of

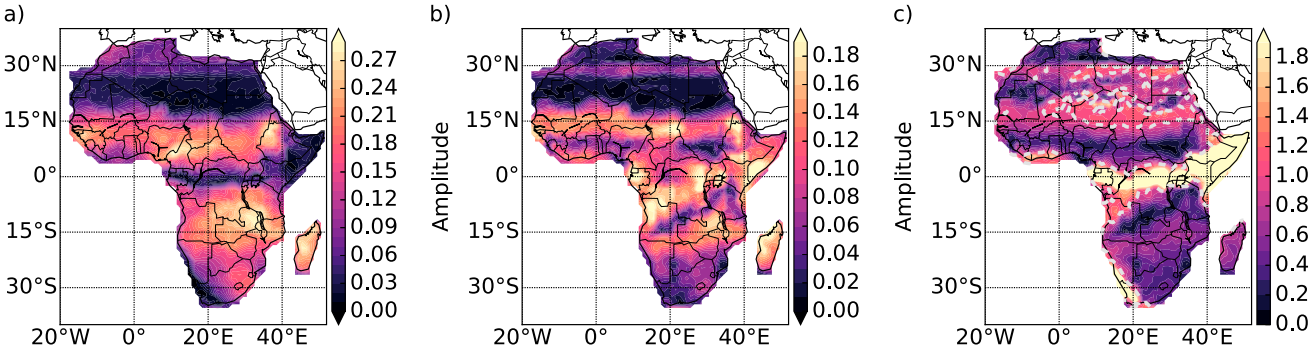

Figure 1. Amplitude of the harmonics at frequency of (a) one and (b) two cycles per year for each grid point in TARCATv2 (1984–2014). (c) The ratio of the amplitudes (b/a). The dashed contour in Figure 1c marks where the ratio is equal to 1.0.

wet seasons per year over Africa, although they used threshold ratios of both 0.75 and 4.0 and monthly rather than daily precipitation data. The method has also been utilized for other applications; *Yang and Slingo* [2001] used Fourier analysis in their examination of the diurnal cycle in convection over the tropics.

Visually, all the data sets appear to show the same patterns and identify broadly similar regions as biannual in agreement with other studies (e.g., the Horn of Africa [*Camberlin et al.*, 2009; *Yang et al.*, 2015b], a zonal equatorial strip extending from Uganda to Equatorial Guinea [*Diem et al.*, 2014], and a small region on the southern West African coastline [*Sultan and Janicot*, 2003; *Liebmann et al.*, 2012; *Herrmann and Mohr*, 2011; *Sylla et al.*, 2010]) suggesting that this method is successfully identifying regions with two wet seasons per year. *Herrmann and Mohr* [2011] defined the number of seasons using monthly precipitation and temperature data and also found a small region on the southern West African coastline and the Horn of Africa have two wet seasons, although they defined the equatorial strip as humid with no seasonal cycle, whereas here it has been defined as having two seasons. *Nicholson* [2000] highlighted a much wider area as having two seasons than that found here yet identified areas with a biannual regime having a rainfall maxima in the austral or boreal summer rather than in transition seasons, as would be expected [*Washington et al.*, 2013]. Comparison of the region shown as having a rainfall maxima in transition seasons in *Nicholson* [2000] with the area that experiences a biannual regime found here gives much better agreement. Figure 1c also shows a high ratio over parts of the Sahara and north Africa, but this is due to low rainfall, as described above. ARCv2, TARCATv2, TRMM, and ERA-I also identify the south west tip of Africa as biannual; this is again thought to be due to the dry climate [*Herrmann and Mohr*, 2011; *Nicholson*, 2000].

The ratio maps for the six data sets were compared using Pearson pattern correlation (PPC) and mean absolute error (MAE). MAE values are between 0.6 and 0.7, with all data sets performing similarly. The PPC coefficients are between 0.16 and 0.63, with all but the correlation between GPCP and ARCv2 (0.16) significant at the 99% level. Examining the pattern correlation for the amplitude of the first and second harmonics individually gave higher correlations, with values of 0.84–0.96 for the first harmonic and 0.63–0.87 for the second harmonic. In summary, using harmonics to determine the number of wet seasons has produced results similar to those in other studies, and all the data sets give consistent results showing a small region on the southern West African Coastline, the Horn of Africa, and the equatorial strip as the biannual regions.

2.2.2. Diagnosing Onset and Cessation for Annual Regimes

The method used to determine the onset and cessation at grid points with an annual regime described here is as in *Liebmann et al.* [2012]. Initially, the period of the year when the wet season occurs, termed the climatological water season, must be determined, to account for those seasons that span calendar years. First, the climatological mean rainfall for each day of the calendar year, Q_i, where i goes from 1 January to 31 December, is computed (red line in Figure 2) and the climatological daily mean rainfall $\bar{Q}$. From this the climatological cumulative daily rainfall anomaly on day d, $C(d)$, is found:

$$C(d) = \sum_{i=1\text{Jan}}^{d} Q_i - \bar{Q} \tag{1}$$

where i ranges from 1 January to the day (d) for which the calculation applies. In this example, $C(d)$ is calculated for each day from 1 January to 31 December. Figure 2 shows ($Q_i - \bar{Q}$) as a blue line and $C(d)$ as a green line.

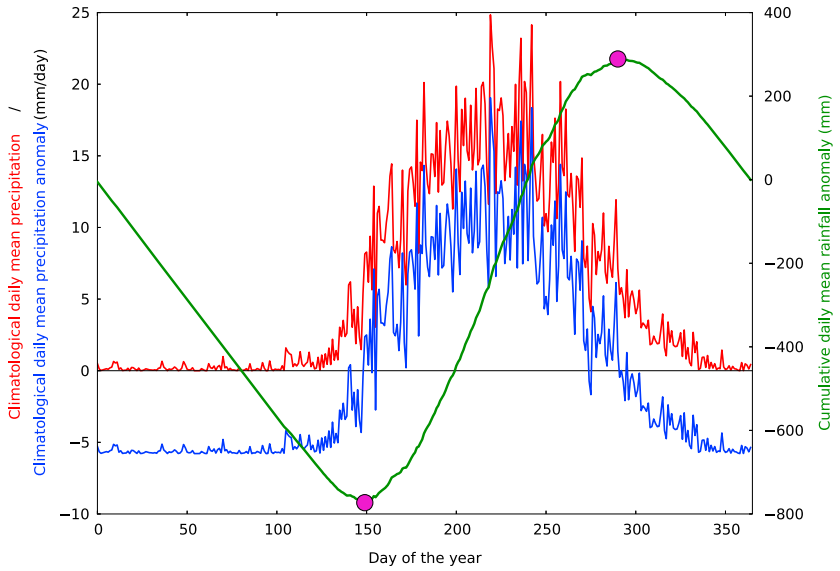

Figure 2. Climatological daily mean rainfall for each day of the year (red), climatological daily mean rainfall anomaly (blue), and climatological cumulative daily mean rainfall anomaly (green) for 9.5°N, 14.5°W from GPCP averaged over 1997–2014. The magenta dots mark the extent of the climatological water season.

The day of the minimum in C marks the beginning of the climatological water season, d_s, and the maximum marks the end, d_e.

In the second stage the onset dates are calculated individually for each year, by computing the daily cumulative rainfall anomaly on day D, $A(D)$:

$$A(D) = \sum_{j=d_s-50}^{D} R_j - \bar{Q} \tag{2}$$

where R_j is the rainfall on day j and j ranges from $d_s - 50$ to the day being considered (D). $A(D)$ is calculated for each day from $d_s - 50$ to $d_e + 50$ for each year. The day after the minimum in $A(D)$ is the onset, as after this the rainfall is persistent in occurrence, duration, and intensity [*Diaconescu et al.*, 2015], and the day of the maximum (after the minimum) is the cessation date. Since the climatological water season may potentially span multiple calendar years the onset and cessation is not computed for the first and last year of each record.

2.2.3. Diagnosing the Onset and Cessation for Biannual Regimes

For points where there are two wet seasons per year, a different method is required in order to determine the periods of the year when wet seasons, or climatological water seasons, occur (Figure 3). This part of the method is proposed for the first time in this paper. The climatological cumulative daily rainfall anomaly $C(d)$ (green line in Figure 3, calculated in the same way as above) for each point is smoothed using a 30 day running mean ($S(d)$, purple line). Minima/maxima in the smoothed curve are detected by identifying days where $S(d)$ is lower/higher than the four preceding days and lower/higher than the four following days (Figure 3a). A number of periods were considered, and 4 days was chosen as it gave enough minima and maxima to identify the season but did not erroneously place minima and maxima midseason. For each minima, the first following maxima is located and is assumed to end that season. The two longest seasons are assumed to be the two seasons of interest. Thus, in Figure 3, the two main seasons are selected, and the other minima and maxima found by the method are discarded. This gives two season start and end dates, d_{s1}, d_{e1}, d_{s2}, and d_{e2}.

These seasons are then considered separately, and the individual onset and cessation dates are found using the second part of the one season method:

$$A(D) = \sum_{j=d_{s1}-20}^{D} R_j - \bar{Q} \tag{3}$$

where R_j is the rainfall on day j and j ranges from $d_{s1} - 20$ to the day being considered (D). $A(D)$ is calculated for each day from $d_{s1} - 20$ to $d_{e1} + 20$, and for each day from $d_{s2} - 20$ and $d_{e2} + 20$, for each year. A shorter

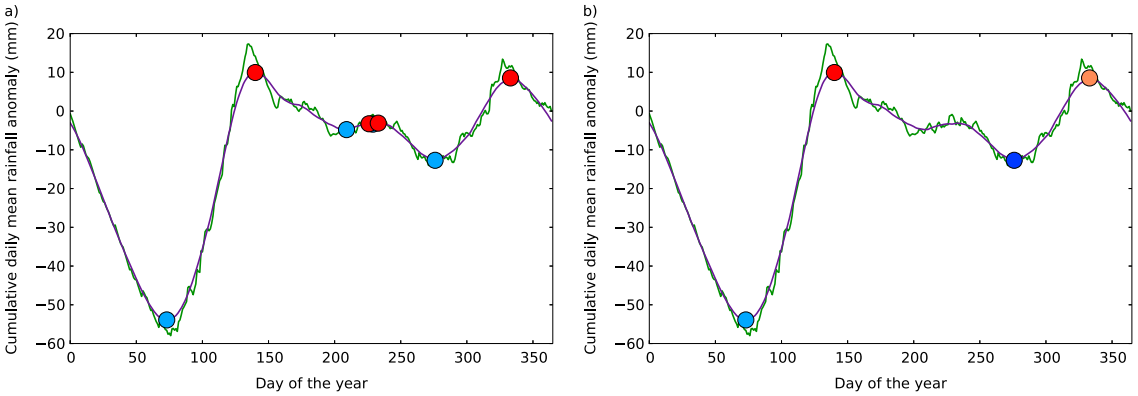

Figure 3. Climatological cumulative daily mean rainfall anomaly (green) and climatological cumulative daily mean rainfall anomaly smoothed using a 30 day running mean (purple) for 34.5°E, 3.5°N from GPCP averaged over 1997–2014. The blue (red) dots in (a) mark all the minima (maxima) found using the method detailed in section 2.2.3. (b) shows just those minima and maxima that mark the beginning and end of the climatological water seasons. The light and dark blue dots in (b) mark the beginning of the two seasons, while the red and orange dots mark the end of the two seasons.

period of 20 days (as opposed to 50 used above) was used to ensure the correct season was captured, as the intervening dry periods between multiple wet seasons may be shorter than 100 days; for example, over the West Africa southern coastal region the little dry season occurs during July and August only. Minima and maxima in $A(D)$ were again used to identify onset and cessation dates.

The first and second seasons were objectively split using the start date of the climatological water seasons; the season that started between 31 May and 27 October was considered to be the second rainy season, and the other was considered to be the first rainy season. The long length of this window is designed to capture the start of the second season over West Africa in August–September and the onset over Kenya in October. Over Kenya and East Africa these are referred to as the "short" rains and "long" rains, respectively, and this terminology is used when discussing this area.

2.3. Regions

Africa was divided into a number of regions (Figure 4). Regions were chosen such that they experienced an annual or biannual regime consistently across all data sets; grid points with conflicting definitions are shaded in pink in Figure 4 and have not been included. Two regions have been excluded; north of 15°N is predominantly arid over the Sahara Desert, so there is no pronounced wet season, and the Mediterranean region shows very large differences between the data sets (shaded in dark purple in Figure 4) due to the dry climate resulting in few data sets giving values here (see Figures S2 and S3 in the supporting information). The biannual region over the Democratic Republic of the Congo, Uganda, and Gabon has also not been considered (shaded in light purple in Figure 4); this region is known to be humid and therefore may not exhibit a dry season in all years [*Herrmann and Mohr*, 2011] and shows large variation between the different data sets (see section 4). Seasonality is less important in such regions, due to higher rainfall totals and more continuous precipitation. A small area covering southern Gabon and the Republic of the Congo, shown in orange as it has an annual regime, was not included as it is separated from region 12 by grid points with conflicting definitions. The regions were also chosen to contain broadly contemporaneous onset and cessation dates. Regions 1–3, 5–7, and 11–17 experience an annual regime (orange in Figure 4), and regions 4 and 8–10 experience a biannual regime (yellow in Figure 4). The mean spatial standard deviation for onset and cessation over each region was computed to confirm spatial homogeneity in each region. With the exception of region 16 (covering central and eastern South Africa), all regions had mean spatial standard deviation for onset of less than 30 days and less than 20 days for cessation. Plotting median cessation against median onset showed good clustering of points by region (not shown), with some outliers for region 16. Thus, the regions were considered satisfactory for this analysis of continental scale patterns, with extra consideration required for region 16. While the majority of South Africa experiences a single wet season during austral summer, the south coast of South Africa experiences rainfall throughout the calendar year, and the western part receives winter rainfall [*Engelbrecht et al.*, 2015; *Weldon and Reason*, 2014]. While exclusion of regions containing conflicting definitions (pink in Figure 4) removes much of the winter rainfall regime, the large variability is likely to be a consequence of the inclusion of differing rainfall regimes. Region 4 is referred to throughout as the West African southern coastal region.

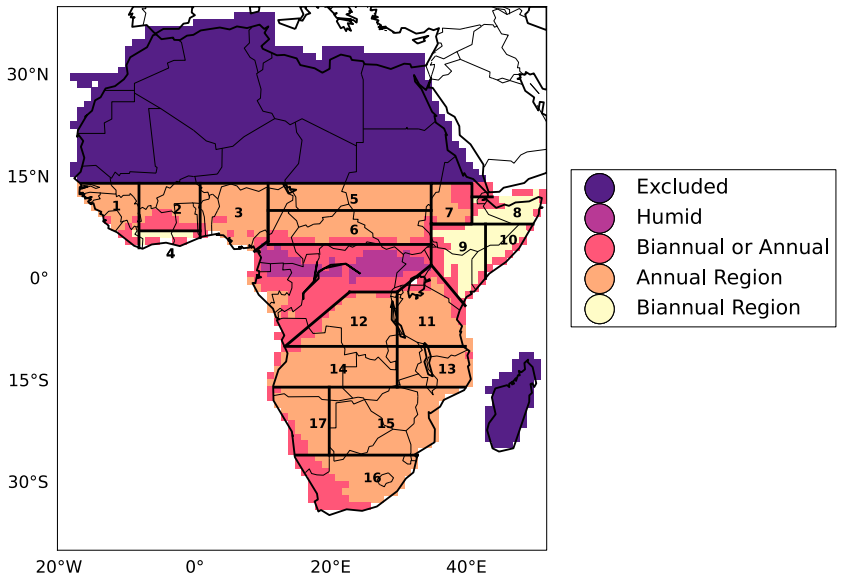

Figure 4. Regions used for analysis (1–17). Dark purple indicates areas excluded, pink indicates regions that are defined as annual and biannual in different data sets, and light purple indicates the humid region of central Africa. Orange regions are annual regime regions, and yellow regions are biannual regions.

3. Physical Relevance of the Seasonality Metric

Previous work has demonstrated the stability of the method described in section 2.2.2 for capturing onset and cessation dates [*Liebmann et al.*, 2012; *Boyard-Micheau et al.*, 2013]. This is further discussed in section 4. Here we assess the physical relevance of this quantity as a metric for seasonality of African rainfall. First, we examine the agreement between our results and two of the main physical drivers of African rainfall, namely, seasonal progression of the Intertropical Convergence Zone (ITCZ) and the West African Monsoon. Second, the consistency with agriculturally based definitions of the seasonal cycle is assessed, via comparison with local, threshold-based onset methods which have been designed with agricultural applicability in mind.

3.1. Movement of the ITCZ

Seasonal progression of the ITCZ, here taken as the band of maximum precipitation and convection, is the main driver of the seasonal cycle of precipitation for the majority of Africa. Our results for the climatological seasonal cycle are compared against published literature on the ITCZ. The focus is predominantly on regions with a biannual regime.

Figure 5 shows the onset of the second and first rains plotted with the onset of the southern and northern single wet seasons, respectively, and the cessation of the second and first rains plotted with the cessation of the northern and southern single seasons, respectively. The contour marked shows the position of the annual/biannual boundary. The progression of the ITCZ appears to be spatially continuous with no marked artificial shifts (e.g., along the annual/biannual boundary) and no large spurious discrepancies between neighboring grid points. This demonstrates that the onset dates identified by the biannual method are compatible with those found using the method for annual regimes. However, rapid progressions (or "jumps") that are present in reality are captured [*Hagos and Cook*, 2007].

During the austral spring the ITCZ travels south, bringing the second rainy season and then the wet season over southern Africa. Figure 5a shows a continuous progression from the onset of the second rains over central Africa and the Democratic Republic of the Congo into the rest of southern Africa, beginning on 27 August on average at 20.5°E, 0.5°S, and later onset in the east and over the Horn of Africa, with onset occurring on 8 October (on average) at 43.5°E, 4.5°N, consistent with the pattern found in *Liebmann et al.* [2012]. The end of the northern wet season progresses zonally southward with the cessation of the second rains following in a similar manner (Figure 5b). The onset of the first rains over the West Africa southern coastal region in the late boreal spring merges well with the onset of the wider West African Monsoon (Figure 5c), and the cessation of the first rains follows the retreat of the rainfall over southern Africa, starting at the Zimbabwe, Mozambique,

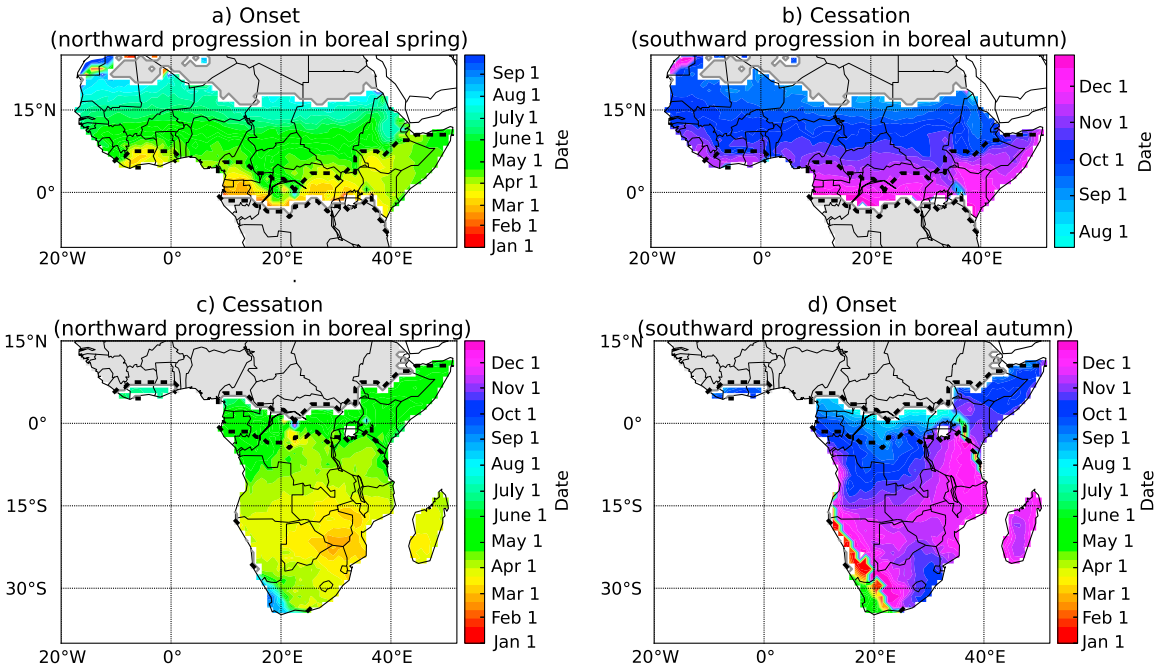

Figure 5. Southward and northward progression of onset and cessation across the annual/biannual boundaries. (a) The northward progression of onset in boreal spring from onset of the first/long rains into onset of the West African Monsoon. (b) The southward progression of cessation in boreal autumn from the cessation of the West African Monsoon into the end of the second/short rains. (d) The southward progression of onset in boreal autumn, from the onset of the second/short rains into the onset of the annual rains over southern Africa. (c) The northward progression of cessation in boreal spring from the end of the annual rains over southern Africa into the end of the first/long rains. These were computed using the GPCP data set over 1998–2013. Grey indicates regions not considered for these plots.

South Africa border on the 4 March, and reaching Equatorial Guinea (10.5°E, 1.5°N) on 23 May (Figure 5d). Both the zonal pattern of onset over West and central Africa, and the radial pattern over southern Africa are well matched and consistent with the first rains onset and cessation.

Figure 6 contains the onset and cessation for the 17 regions shown in Figure 4. These results are consistent with published onset and cessation dates in the literature for East Africa [*Ngetich et al.*, 2014; *Camberlin et al.*, 2009], the West Africa southern coastal region [*Thorncroft et al.*, 2011; *Adejuwon and Odekunle*, 2006; *Nguyen et al.*, 2011; *Sultan and Janicot*, 2003; *Nicholson*, 2013], and southern Africa [*Shongwe et al.*, 2015; *Kniveton et al.*, 2009].

3.2. Consistency With West Africa Monsoon Dynamics

In West Africa the seasonal cycle is driven by the monsoon. Figure 6a shows the mean onset and cessation for regions 1–6 (see Figure 4) from all six data sets. Region 4 (West Africa southern coastal region) experiences two wet seasons per year, 1–3 and 5–6 experience an annual regime.

The onset of the first rains and cessation of the second rains over the West Africa southern coastal region merges well with the wider onset and cessation over West Africa (Figures 5b and 5c). The onset of the West African Monsoon is comprised of two stages; the preonset and onset [*Sultan and Janicot*, 2003]. During late boreal spring the Intertropical Front (ITF), which marks the northern limit of the southwesterly monsoon winds, migrates northward, while the ITCZ remains south of West Africa. This initiates local convection, and the beginning of the first wet season on the southern coastline, around early April. Onset over region 4 is around 17 March to 27 April, consistent with the mid-April onset of the coastal phase found in *Thorncroft et al.* [2011].

Later, during the boreal summer, the ITCZ abruptly shifts north, bringing the onset of the monsoon rains across the rest of West Africa. At this time, there is a decline in the rainfall along the coast, known as the little dry season, which occurs from mid-July into August [*Adejuwon and Odekunle*, 2006]. After the onset in region 4, onset commences in the surrounding regions (1–3 and 5–6), and the first wet season over the West Africa southern coastal region ends around 25 June to 5 July (Figure 6a). *Adejuwon and Odekunle* [2006] found the start of the little dry season over SW Nigeria between 15 and 25 July, *Sultan and Janicot* [2003] showed it beginning

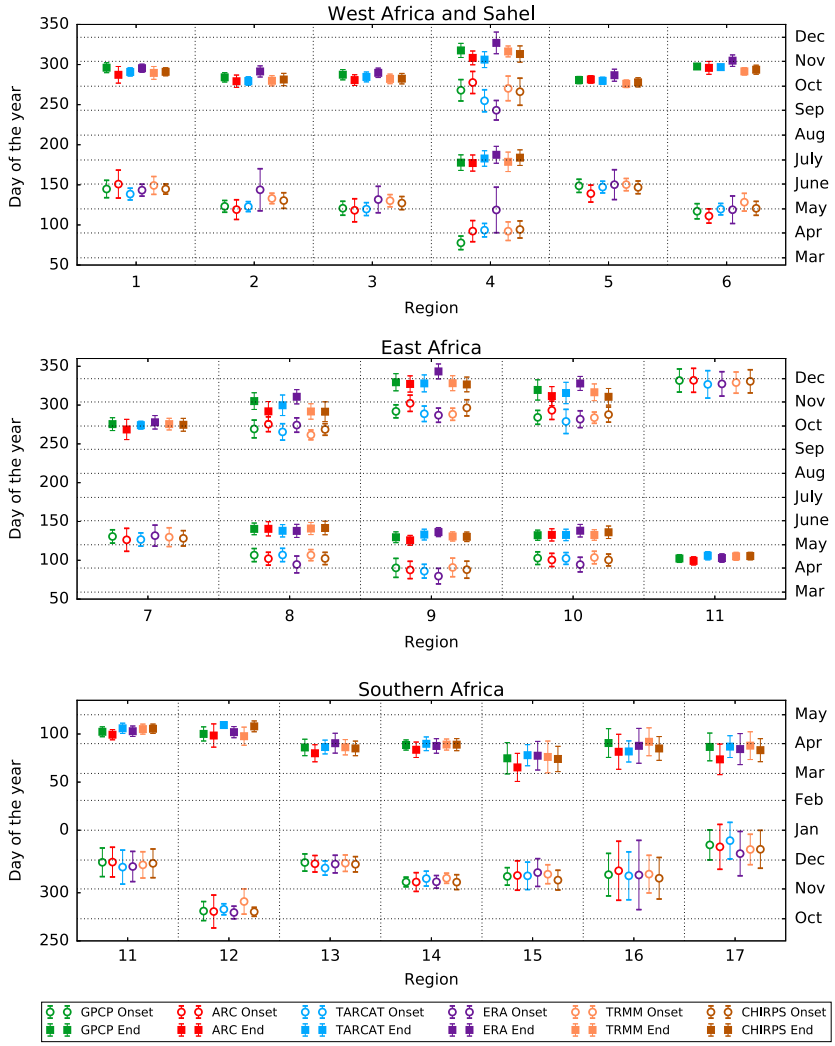

Figure 6. Mean and standard deviation of the mean onset and cessation date for each data set over the regions in western (regions 1–6), eastern (regions 7–11), and southern (regions 11–17) Africa (a,b,c respectively).

around early July at 5°N, and *Nguyen et al.* [2011] found the demise of the coastal rainfall occurred on 26 June, consistent with the dates shown in Figure 6a. Successfully capturing the little dry season is a strength of this method. At the end of the boreal summer, as the monsoon retreats equatorward, the wet season terminates over West Africa and the coastal region experiences a second rainfall peak from August/September to early November [*Sultan and Janicot*, 2003; *Nicholson*, 2013; *Thorncroft et al.*, 2011].

Figure 6a shows that as the monsoon season ends over regions 1–3 and 5–6, a second wet season occurs over the West Africa southern coastal region. *Zhang and Cook* [2014] found monsoon demise over the Sahel ranging from 5 October to 30 October, consistent with the October cessation dates found for regions 1–3 and 5–6 in Figure 6a. They also noted a later demise in western coastal Sahel, in comparison with central and eastern regions, also apparent in our results, which can be seen by comparing the cessation dates over Sierra Leone with the same latitude in Nigeria (Figure 5b). The second wet season over the West Africa southern coastal region starts around 30 August – 3 October, consistent with *Sultan and Janicot* [2003] who find a start around August/September and *Adejuwon and Odekunle* [2006] who find the end of the little dry season between 29 August and 8 September. The similarity between our results and those of *Sultan and Janicot* [2003] is particularly noteworthy, given their use of station-based rainfall. The end of this second wet season marks the end of the West African Monsoon, around 1–22 November (Figure 6a), which can be seen in Figure 5b.

3.3. Comparison With Other Methods for Identifying the Onset

The previous subsections have demonstrated that this method identifies seasons that are consistent with dynamical drivers of African rainfall. In order to evaluate consistency with agricultural definitions of the seasonal cycle, we compare our results against two other onset methods, calibrated locally and designed to identify the start of the growing season. The first method is that of *Marteau et al.* [2009], which is based on a threshold of 20 mm being exceeded over 1–2 days, with no 7 day dry period in the following 20 days. The second method is a combination of *Issa Lélé and Lamb* [2010] and *Yamada et al.* [2013], which requires a rainfall rate of large enough magnitude to be societally useful (3–4 mm/d) over a longer period (14 days).

This comparison was completed over all grid points in 9°N–15°N and 0°–20°W, which is the area used in *Marteau et al.* [2009]. Since both local onset methods do not consider the period prior to 1 May, the same limit was applied to all methods, for the purpose of this comparison. The agreement between the two local onset methods was good, with a PPC coefficient of 0.97 and an MAE value of 12.5 days (on average). Agreement with the method presented here was also good, with correlation values of 0.84 and 0.9 for *Marteau et al.* [2009] and *Issa Lélé and Lamb* [2010], respectively. The MAE values were 16.8 days and 8.41 days (on average) for *Marteau et al.* [2009] and *Issa Lélé and Lamb* [2010], respectively. This indicates that the onset dates given here do coincide with indigenous methods. The similarity of values found when comparing the two local methods and those when this method was used confirms that the differences are not much larger when the method of cumulative anomalies is used.

In this section it has been demonstrated, through comparison with known physical drivers of African seasonal rainfall, and previously used onset methods, that the method for determining the onset and cessation of the wet season detailed above is able to capture the correct physical progression of the seasonal rainfall across both annual and biannual regions of Africa.

4. Evaluation Over a Range of Data Sets

This method is designed to account for systematic bias in variability and amount so that identified discrepancies between data sets relate primarily to differences in their representation of the seasonality of rainfall. In this section we assess these features by comparing onset and cessation dates from six data sets of African precipitation. Mean onset and cessation dates and their temporal variability across all data sets are displayed in Figure 6 for western, eastern, and southern Africa. Temporal variability in onset and cessation is quantified as the interannual standard deviation of the mean date across each region for each data set, depicted in Figure 6 as error bars. Figures containing the mean onset and cessation for each of the six data sets are included in the supporting information; the median value across all six data sets are shown in Figures 7, 8a–8b and 8c–8d for annual regimes, the first/long rains and the second/short rains, respectively. On Figures 7- 8 crosses indicate grid points where more than one of the data set means were outside the range (median $\pm$ 1 standard deviation), where the standard deviation is defined uniquely for each grid point, and is the mean standard deviation of onset/cessation over all six data sets. Regions where the standard deviation of daily rainfall was less than 1 mm/d were excluded, as this indicates a dry regime with no marked wet and dry seasons. Annual and biannual regimes have been considered separately.

4.1. Annual Rainfall Regime

Figures 6 and 7 generally indicate good agreement between the onset and cessation dates in the different data sets. The pattern over the coast of southwest South Africa and Namibia is one region of difference between the data sets (Figure 7); the data sets differ here in their annual/biannual categorization; hence, it is shaded pink in Figure 4 and has not been included in the regional analysis. In general, Figure 7a indicates an onset date in January for the northern part of this coastal strip, and April–May for the southern part consistent with the rainfall maxima in May–June and March for the southern and northern parts of this region, respectively, found in *Nicholson* [2000]. The Mediterranean coastline and parts of the Sahara contain regions of disagreement, where the wet season is poorly defined. Mean onset for annual regions (regions 1–3, 5–7, and 11–17; Figure 6) shows some inter-data set variation between the onset dates, including a later onset over region 2 in West Africa in ERA-I (see section 4.3), and TRMM appears to have a later mean onset over region 12, but for the most part, the mean onset date for each region is fairly consistent for the different data sets. Consistent spatial patterns across the data sets are confirmed by high (>0.82) PPC coefficients (below diagonal in Table 2), found to be statistically significant at the 99% level, despite the high autocorrelation [*Wilks*, 2011; *Adams and Lawrence*, 2014]. MAE values (above diagonal in Table 2) confirm the good agreement with values

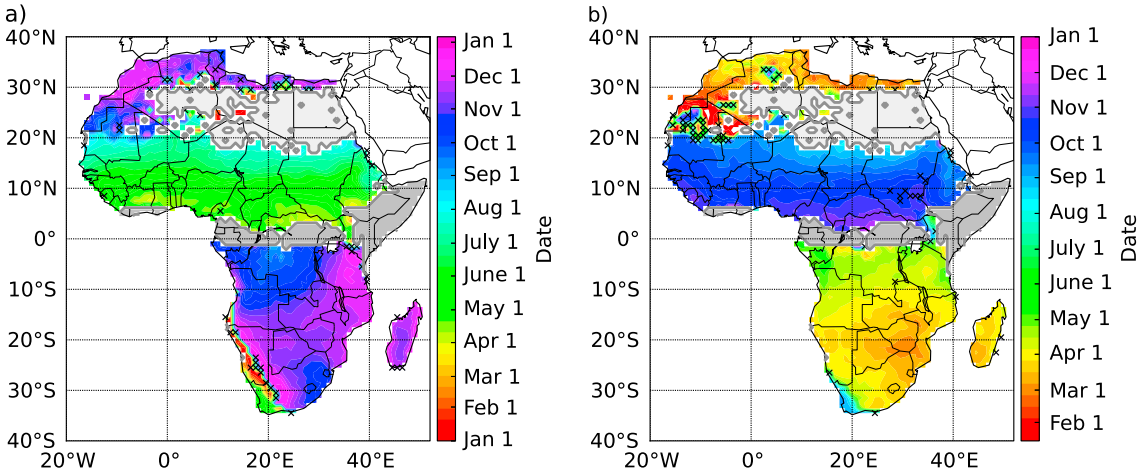

Figure 7. Median of the (a) mean onset and (b) mean cessation date for annual regime regions over all data sets. Stippling indicates where there is more than one mean value outside the median ± 1 standard deviation, where the standard deviation used is the mean of the standard deviation in onset/cessation at that grid point over all six data sets. Dark grey indicates biannual regions, and pale grey indicates dry regions.

of 10–17 days with the highest MAE values associated with ERA-I. Interannual variability (Figure 6) is generally consistent across data sets, with the largest values consistently found over regions 15, 16, and 17. Although the southwest coastal strip is excluded (shaded pink in Figure 4), this is likely the result of the inclusion of different rainfall regimes and drier climates, especially across South Africa [*Engelbrecht et al.*, 2015; *Weldon and Reason*, 2014].

Good agreement is also apparent in cessation dates from different data sets over regions with an annual regime (Figures 6 and 7b). Notable exceptions include early cessation in ARCv2 over regions 15 and 17 and to a lesser extent over regions 1, 7, 13, and 14 and late mean cessation in ERA-I over regions 2, 5, and 6. The individual mean cessation plots confirm the early cessation in ARCv2 over southern Africa, (see Figure S3b in the supporting information). High (>0.96), statistically significant (at 99% level) PPC coefficients (below diagonal in Table 3) confirm consistent spatial patterns, and good agreement is demonstrated in low MAE values of 5–10 days (above diagonal in Table 3). Interannual variability is generally lower for cessation than onset (Figure 6), and is again generally consistent across data sets, with the largest values over regions 15–17.

Overall, there is good agreement between the onset and cessation found in the different data sets in regions with an annual regime, demonstrating that all the data sets used contain a consistent representation of the seasonal cycle, as defined using the method above. This suggests that all the different satellite based precipitation data sets are accurately capturing the same patterns of annual rainfall progression over Africa.

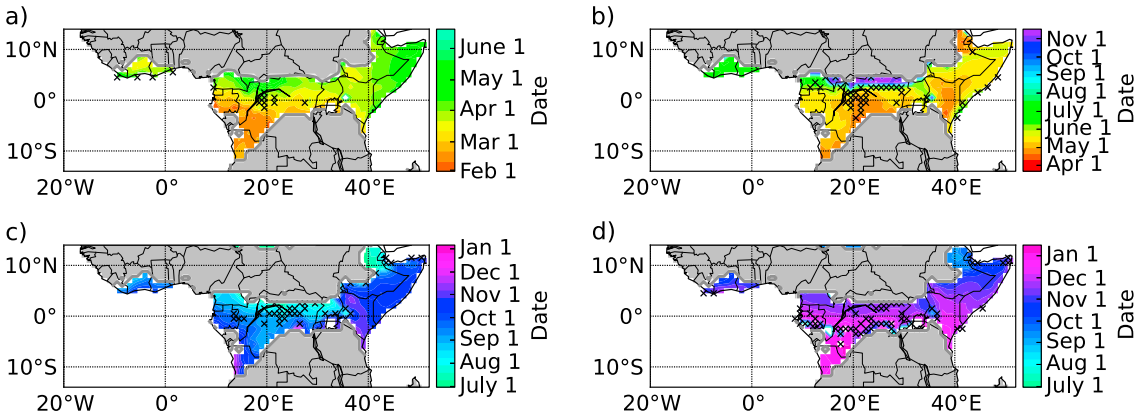

Figure 8. Median of the mean onset and cessation dates for the (a, b) first/long and (c, d) second/short rains over all data sets. Stippling indicates where there is more than one mean value outside the median ± 1 standard deviation, where the standard deviation used is the mean of the standard deviation in onset/cessation at that grid point over all six data sets. Grey indicates annual regimes.

Table 2. Comparison of Mean Onset Date Between the Six Data Sets Over Annual Regime Regions[a]

	TARCATv2	ARCv2	GPCP	TRMM	CHIRPS	ERA-I
TARCATv2		14.02	11.51	14.27	11.16	16.38
ARCv2	0.89		17.71	17.97	15.68	17.16
GPCP	0.91	0.82		13.69	10.64	15.37
TRMM	0.90	0.85	0.88		10.97	15.17
CHIRPS	0.92	0.85	0.90	0.91		11.20
ERA	0.86	0.87	0.86	0.87	0.93	

[a]Below the diagonal is the Pearson pattern correlation (PPC) coefficient, and above the diagonal is the mean absolute error (days).

The reanalysis data set (ERA-I) has been found to have some discrepancies over certain regions (e.g., region 2; see section 4.3) but mostly shows good agreement with the observational data sets.

4.2. Biannual Rainfall Regime

For the most part, the data sets agree well for the biannual regions (Figure 8), with central Africa exhibiting the largest disagreement, while the Horn of Africa and the West Africa southern coastal region contain few points of disagreement. Because this is the first time this method has been applied to biannual rainfall, the next sections provide discussion of the three regions that experience more than one season per year, namely, central Africa, East Africa, and the West Africa southern coastal region.

4.2.1. Central Africa

The majority of regions of disagreement in Figure 8 reside within inland equatorial Africa, with the disagreement in timing of the onset and cessation here related to several factors. First, central Africa experiences a humid climate, with an ill-defined dry season [*Herrmann and Mohr*, 2011], although some studies point out that there are maxima of rainfall in November and March/April [*Washington et al.*, 2013; *Nikulin et al.*, 2012]. In regions, such as this, which are humid all year round, studies of rainfall seasonality are of limited interest. Differences between rainfall estimations in observational data sets over central Africa may result from variations in the inclusion of rain gauge measurements [*Maidment et al.*, 2015]. ERA-I overestimates rainfall over central Africa when compared with both Global Precipitation Climatology Centre precipitation data set [*Paeth et al.*, 2011; *Dee et al.*, 2011] and GPCP [*Nikulin et al.*, 2012]. In addition to large rainfall magnitude differences [*Washington et al.*, 2013], studies have also reported on discrepancies in the phase of the annual rainfall pattern over central Africa. *Sylla et al.* [2010] found that ERA-I does not correctly represent the double peaked seasonal structure and December–January dry season over North and South Equatorial Central Africa, respectively. Over the Congo Basin, *Washington et al.* [2013] showed that TRMM, TAMSAT, and ERA-I all capture the double-peaked pattern, but all three exhibited timing differences. Overall, disagreement in onset and cessation dates found over this region is likely due to significant differences in the data sets.

4.2.2. East Africa

Figure 8 only exhibits disagreement over East Africa (here taken to comprise regions 8–10) on coastlines or the biannual/annual boundary regions, where the two seasons may be less well defined. Figure 6b supports this conclusion of good agreement between the data sets for the long rains over regions 8–10, both in terms of

Table 3. Comparison of Mean Cessation Date Between the Six Data Sets Over Annual Regime Regions[a]

	TARCATv2	ARCv2	GPCP	TRMM	CHIRPS	ERA-I
TARCATv2		8.21	6.41	7.67	5.65	8.91
ARCv2	0.99		8.85	10.49	7.39	10.29
GPCP	1.00	0.97		6.85	5.12	7.39
TRMM	0.99	0.96	0.98		5.04	8.71
CHIRPS	1.00	0.99	1.00	1.00		7.36
ERA	0.99	0.99	0.99	0.99	1.00	

[a]Below the diagonal is the Pearson pattern correlation (PPC) coefficient, and above the diagonal is the mean absolute error (days).

the mean date, and the consistently low interannual variability. The PPC coefficients and MAE values for both onset and cessation confirm this; MAE values range between 3 and 11 days (3–6 days if ERA-I is excluded), and PPC coefficients are all above the threshold to be significant at the 95% confidence level (results not shown).

The differences are larger for the short rains (Figures 8c, 8d, and 6b) but mostly small in magnitude. For the cessation, all the data sets but ERA-I are consistent in terms of mean cessation date and interannual variability, confirmed by MAE values of 4–8 days when ERA-I is excluded (4–32 days with ERA-I), and PPC coefficients above the threshold to be significant at the 95% confidence level (results not shown). For the onset, ARCv2 seems to give marginally later onset dates, possibly due to the underestimation of ARCv2 rainfall over the Ethiopian Highlands and the surrounding region, particularly from June to September [*Awange et al.*, 2016; *Young et al.*, 2014]. *Young et al.* [2014] found that over eastern Ethiopia ARCv2 contained the lowest rainfall for the June–December period, when compared with gauges, TRMM, CMORPH (CPC MORPHing technique precipitation), and TAMSAT, and only exhibited a marginal increase in rainfall during the short rains season in southeastern Ethiopia. Despite this, the PPC coefficients for the onset are above the threshold to be significant at the 95% confidence level, and MAE values range between 6 and 13 days, indicating that ARCv2 is not a large outlier.

4.2.3. West Africa Southern Coastal Region

Agreement of onset/cessation dates is generally reasonable over the West Africa southern coastal region (Figure 8), but larger variations are found for the second season (Figure 6a). For the first season, the main difference is in the onset; GPCP and ERA-I give mean onset dates of 18 March and 24 April, respectively, with the others all occurring between 1 and 3 April. ERA-I also contains large interannual variability in the onset (Figure 6a). MAE values range from just 5–10 days when GPCP and ERA-I are excluded but increase to 5–17 days and 5–40 days when just GPCP and both GPCP and ERA-I are included, respectively. Agreement in cessation is better, with MAE values of 2–11 days for all data sets (results not shown).

For the onset of the second season, ERA-I gives the earliest cessation date on 30 August, followed by TARCATv2 on 10 September, with the other data sets giving mean onset dates between 22 September and 3 October (Figure 6a). This large difference in onset date is found in the MAE values with values of 4–10 days when TARCATv2 and ERA-I are excluded but increasing to 21 days when TARCATv2 is included and 33 days when ERA-I is included. Cessation is only marginally less variable, with earliest dates in TARCATv2 and ARCv2 at the beginning of November, and latest cessation in ERA-I at the end of November. MAE values range between 3 and 11 days when ERA-I is excluded and 3 and 20 days when ERA-I is included (results not shown).

The results here are less consistent than those for East Africa and for annual regimes, with larger differences found between the TARCATv2, ERA-I, and GPCP data sets. Differences in TARCATv2 are not unexpected, given the overall rainfall underestimation in TARCATv2 along the West African Coastline [*Maidment et al.*, 2014; *Tarnavsky et al.*, 2014]. *Diaconescu et al.* [2015] found GPCP had more days with rainfall >10mm and longer continuous wet periods over this region than TRMM, ARCv2, and ERA-I, which may be related to the earlier onset found in the first rains in GPCP. ARCv2 exhibits larger variability over region 1; time series in the supporting information (Figure S6c) attributes this to an excursion in both onset and cessation in ARCv2 over 2001–2007, likely due to a dry bias during 2001–2007 and may relate to inhomogeneity in the rain gauge record [*Maidment et al.*, 2015]. Generally, the largest differences over the West Africa southern coastal region are related to ERA-I and are explored in section 4.3.

4.3. Differences Between ERA-I and Other Data Sets Over West Africa

ERA-I is a reanalysis data set; hence, rainfall is calculated differently to observational data sets. While ERA-I assimilates observations, model parametrizations are required to generate cloud and rainfall, and changes in observing systems can introduce spurious variability in the hydrological cycle [e.g. *Dee et al.*, 2011]. In general, reanalysis data would not be expected to exactly represent observational data. For the most part, Figures 6–8 indicate that ERA-I performs well over southern Africa, exhibits some timing differences over Eastern Africa, and contains notable disagreements over western Africa. Given the nature of the data set, we therefore have low confidence in the variability in ERA-I onset/cessation dates over West Africa, which are at odds with the other data sets.

Time series for regions 2 and 4 (Figure 9) indicate a trend toward later onset by ERA-I (first rains in region 4), which explains the large variability shown in Figure 6a. In addition, ERA-I exhibits later cessation (second rains in region 4; Figure 6a); Figure 9 confirms that this bias is present throughout the time series for region 2 but

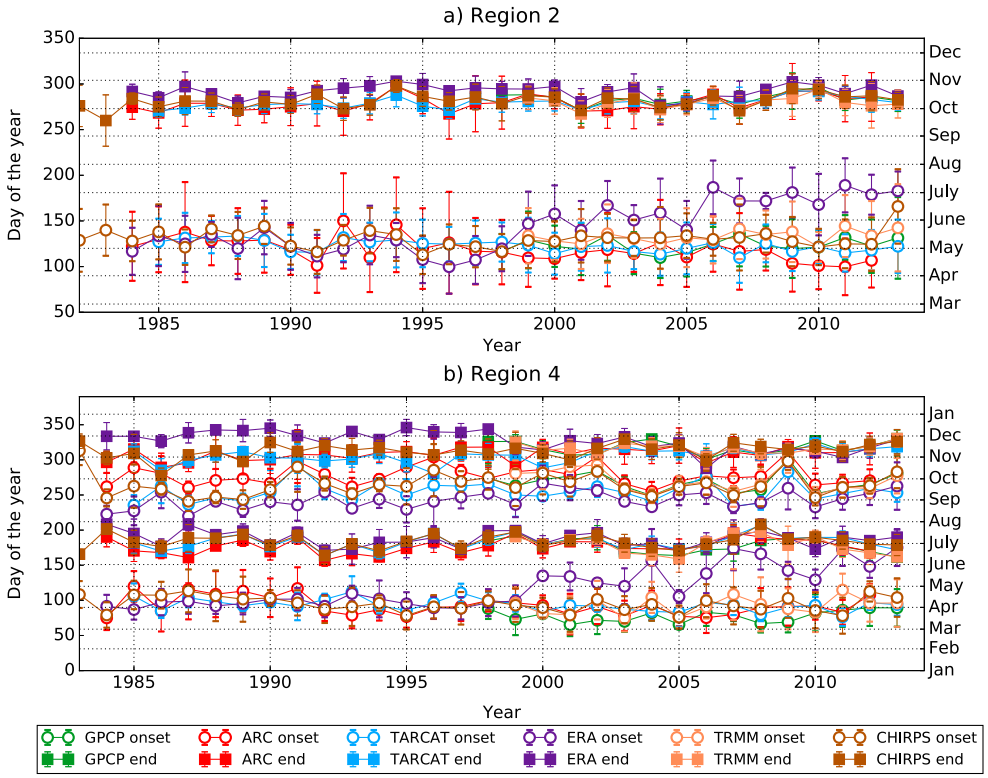

Figure 9. Time series of mean onset and cessation over regions (a) 2 and (b) 4. Different colored lines indicate different data sets. The error bars show the standard deviation in onset/cessation across the region at each time.

only prior to 2000 for region 4 (second rains). The little dry season (the period between the two wet seasons over region 4) is much shorter in ERA-I than the other data sets.

Other studies have indicated that precipitation amount and variability in ERA-I differs from observational data sets over West Africa (and other areas, e.g., central Africa [*Nikulin et al.*, 2012; *Sylla et al.*, 2010]). Although the large-scale features of the West African Monsoon are captured, a lack of northward propagation of precipitation results in an ERA-I overestimation of precipitation along the coast and an underestimation further north [*Diaconescu et al.*, 2015; *Paeth et al.*, 2011; *Nikulin et al.*, 2012; *Hill et al.*, 2016]. A weaker first rainfall maxima along the coast [*Diaconescu et al.*, 2015; *Nikulin et al.*, 2012], matched by a shorter first season resulting from the later onset in our results, suggests that this rainfall overestimation is associated with the second wet season. The failure of ERA-I to propagate the rain band north over the Sahel and consequential southerly location of the rainfall maxima (compared with observations [*Nikulin et al.*, 2012]), results in the reduced little dry season and earlier onset of the second season found here. The later end of the second season is due to the overestimation of rainfall in this region [*Nikulin et al.*, 2012].

Additionally, ERA-I fails to reproduce the observed interannual variability in precipitation [*Sylla et al.*, 2010], with *Nikulin et al.* [2012] identifying an artificial declining trend in precipitation, consistent with the progressively later onset in ERA-I found in our results, which gave rise to larger interannual variability.

Given that the method described here is able to capture the physical progression of the ITCZ throughout Africa (section 3), including the behavior associated with the West African Monsoon, these discrepancies in ERA-I indicate that this reanalysis data set is not correctly representing the West African Monsoon and little dry season, as found in other studies [*Nikulin et al.*, 2012].

5. Example Application: Interpretation of Interannual Variability Over East Africa

Consistency with known physical drivers (section 3), and good agreement across data sets (section 4), establishes confidence in the method. An example of how the method can be used to analyze interannual

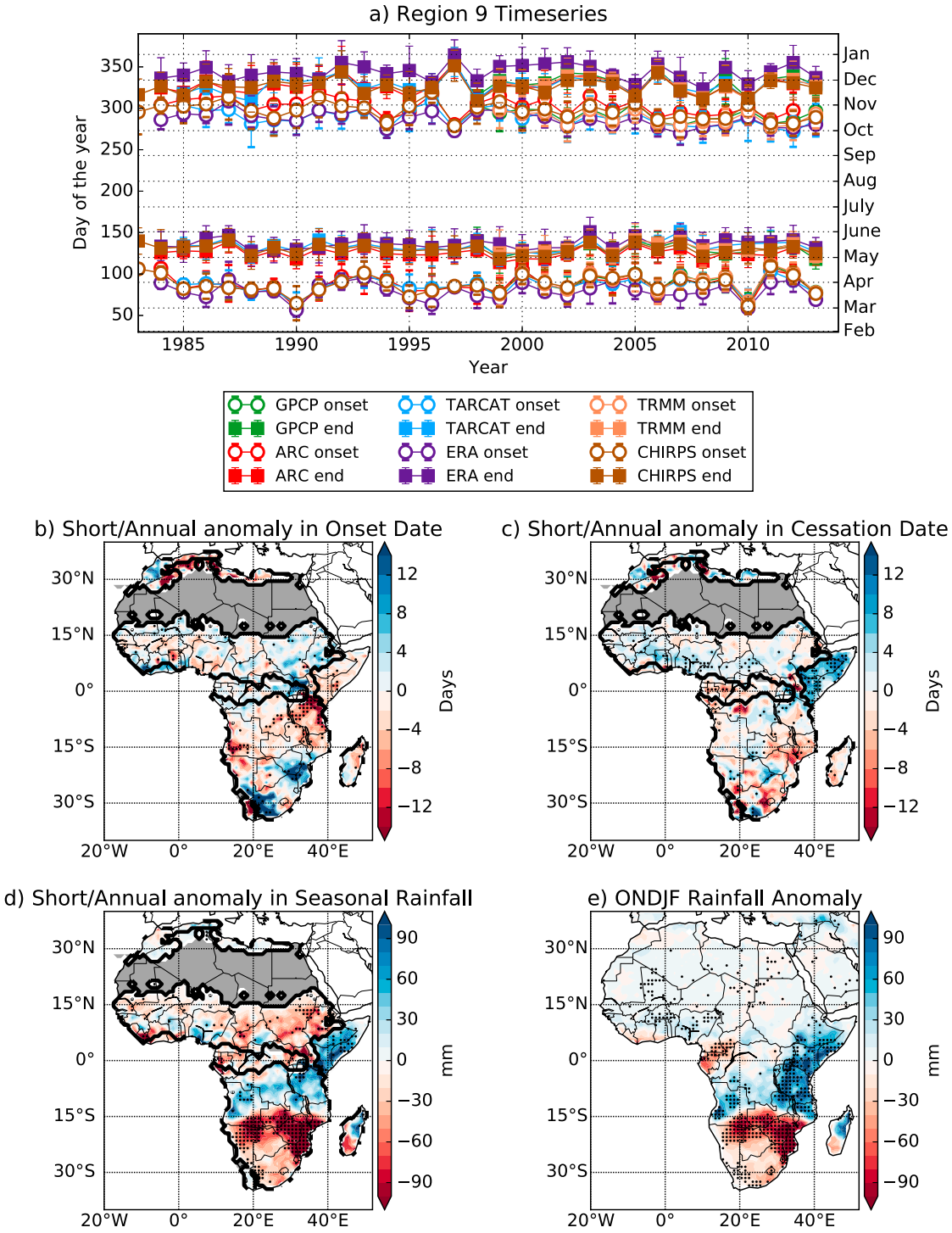

Figure 10. Impact of El Niño on onset/cessation. (a) Time series of mean onset and cessation for long/short rains (bottom/top) over region 9. The error bars show the standard deviation in onset/cessation across the region at each time, with different data sets shown in different colors. (b–d) Composite of onset, cessation, and wet season rainfall, respectively, in El Niño years for annual rains and short rains minus the mean over 1982–2013, computed using CHIRPS data. The black contour marks the biannual/annual boundary. The El Niño years included were 1982, 1986, 1987, 1991, 1994, 1997, 2002, 2004, 2006, and 2009. The grey area indicates a dry regime. (e) October–February (ONDJF) rainfall anomaly in El Niño years (CHIRPS).

variations in onset and cessation over East Africa, detailed in this section, highlights potential applications and usability.

Over East Africa seasons of reduced length indicate lower rainfall [*Philippon et al.*, 2015; *Camberlin et al.*, 2009] and correspond with well-known drought years. A very brief short rain season in 2010 (region 9, Figure 10a; regions 8 and 10, Figure S7) reflects the failure of the 2010 short rains, which, coupled with the reduced long rains in 2011 (Figures 10a and S7), led to drought and famine over East Africa [*Lott et al.*, 2013; *Yang et al.*, 2014; *Hoell and Funk*, 2014]. Failure of the 2005 short rains [*Hastenrath et al.*, 2007] is also discernible in Figure 10a.

Despite the lower interannual variability in the long rains (compared with the short rains [*Camberlin et al.*, 2009]), dry long rains in 1984, 1993, and 2000 and wetter long rains in 1990 [*Philippon et al.*, 2015] are apparent as shorter and longer seasons, respectively, in Figure 10a (and Figure S7). Additionally, the premature end of the long rains in 2004, and early beginning in 2010, is also found by various Kenyan Institutes [*USAID FEWS NET*, 2004; *Kenya Food Security Steering Group (KFSSG)*, 2010]. Correct representation of previously identified rainfall features in the time series (Figures 10a and S7) for all data sets confirms that the method is accurately identifying interannual fluctuations in the wet seasons, and overall, all six data sets have a good representation of the interannual variability in the biannual regions of East Africa.

East African rainfall responded strongly to the 1997–1998 El Niño event, with weaker short rains in 1996 and long rains in 1997, followed by heavier short rains in 1997 immediately preceding the peak of the event, which generated floods across the region [*Black et al.*, 2003]. Immediately following the peak, the 1998 long rains were wetter than usual, followed by drier short rains in the boreal autumn [*Hoell and Funk*, 2014; *Black et al.*, 2003; *Philippon et al.*, 2015]. Overall, it is expected that positive phases of the El Niño Southern Oscillation result in enhanced rainfall, while negative phases result in lower rainfall [*Black et al.*, 2003]. Reduced short rain seasons in 1996 and 1998 for regions 8–10, with a longer season in 1997 (Figures 10a and S7), imply that patterns recorded here match expected behavior across the Horn of Africa. El Niño conditions in 1986 and 1987 also resulted in reduced short rains, consistent with *Philippon et al.* [2015].

One advantage of a continental-scale method for determining onset and cessation, applicable to annual and biannual regimes is the ability to analyze the wider scale variations in seasonality. As an example, and following the findings above, the impact of El Niño upon both the annual rains and short rains was assessed (Figures 10b–10e). The well-documented boreal winter dipole in rainfall anomaly, with higher rainfall totals over 0–15°S and the Horn of Africa and the opposite between 15°S and 30°S (Figure 10e) [*Cook*, 2001; *Camberlin et al.*, 2001; *Kyte et al.*, 2006] is clearly captured in the seasonal rainfall (rainfall between onset date and cessation date) for short rains and annual regimes (Figure 10d). The anomaly is more pronounced over the Horn of Africa in Figure 10d compared to Figure 10e, demonstrating the value of the method extension for biannual regimes. Lower rainfall over 15°S and 30°S is colocated with later onset dates (Figure 10b) and a consequentially shorter season. Higher rainfall to the north is related to longer seasons; however, this results from an earlier onset over the annual regime region (Figure 10b), with onset of the annual rains 9 days earlier over region 11 (Tanzania) in El Niño years, but a later cessation of the short rains (7 days later on average) across the Horn of Africa (Figure 10c). In addition, the rainfall anomaly extends across the continent, but the onset responses are more pronounced east of 20°E. Over West Africa and the Sahel rainfall variations are not clearly associated with changes in seasonal timing. Overall, Figure 10 shows how applying this method over the whole of Africa clearly highlights the spatial patterns in rainfall teleconnections with El Niño.

6. Discussion and Conclusions

A modified method for determining the onset and cessation of the wet season over Africa was proposed and assessed using six observational and reanalysis data sets of African precipitation. The compatibility with known physical drivers of African seasonal rainfall; strong agreement between the different satellite-based precipitation data sets, in both the mean and temporal variations; and consistent features found across both rainfall regimes establish confidence that this method (section 2) successfully captures the annual progression of rainfall across Africa and the beginning and end of the wet season for both regions with one wet season per year, and regions with two wet seasons per year. The onset and cessation are key parameters in

understanding the impact of changes in the seasonal cycle on agriculture [*Boyard-Micheau et al.*, 2013]; and thus, this method provides a foundation on which variability and change in the growing season can be investigated. Its dependence solely on daily rainfall and mean climatology, and proven ability to capture physical patterns, also makes it a suitable metric for analysis of variability and change in rainfall dynamics.

The following conclusions have been reached:

1. Patterns of onset and cessation dates, produced by this method were found to be consistent with known physical drivers of African seasonal precipitation, namely, the ITCZ and the West African Monsoon, as well as agricultural onset methods. Continuous progression of onset and cessation dates across annual/biannual boundaries and consistency between both the detection methods for annual and biannual regions increase confidence in the method. Correct capturing of the little dry season along the West Africa southern coastal region [*Adejuwon and Odekunle*, 2006] is a strength of this method.
2. Patterns of onset and cessation are as found by *Liebmann et al.* [2012] and others [*Oguntunde et al.*, 2014; *Tadross et al.*, 2005; *Mugalavai et al.*, 2008; *Ngetich et al.*, 2014]. Over West Africa, onset and cessation progress in a zonal manner [*Oguntunde et al.*, 2014; *Fitzpatrick et al.*, 2015], whereas over southern Africa onset spreads southeast and northwest simultaneously, and cessation expands radially from the Zimbabwe/ Mozambique/ South Africa border [*Tadross et al.*, 2005].
3. Satellite-based data sets generally agreed in their representation of the seasonal cycle in African rainfall, indicated by PPC coefficients and MAE values, particularly for regions with an annual rainfall regime and the biannual region of East Africa.
4. The largest discrepancies were found in central Africa due to general data set disagreement resulting from the low rain gauge density and generally humid climate with lack of pronounced dry seasons [*Washington et al.*, 2013; *Maidment et al.*, 2015; *Herrmann and Mohr*, 2011]. In regions, such as this, where there is rain all year round, this type of analysis is, in any case, of limited interest.
5. TARCATv2, GPCP, and ARCv2 exhibit differences in the timing of the two wet seasons over the West Africa southern coastal region. TARCATv2 is known to have discrepancies in this region [*Maidment et al.*, 2014; *Tarnavsky et al.*, 2014] and differences have also been found in GPCP [*Diaconescu et al.*, 2015]. The excursion in ARCv2 over 2001–2007, which leads to larger variability, is likely due to a dry bias during 2001–2007, possibly related to inhomogeneity in the rain gauge record [*Maidment et al.*, 2015].
6. Timing errors in the ERA-I reanalysis over the West Africa southern coastal region and East Africa, and a trend toward later onset over West Africa not seen in observational data sets, suggest that while ERA-I has a good representation of the seasonal cycle over annual regime regions, its capturing of biannual seasonal regimes is less robust. ERA-I discrepancies over West Africa are well established [*Diaconescu et al.*, 2015; *Paeth et al.*, 2011; *Nikulin et al.*, 2012] and may indicate that the model precipitation field is not reliable here, consistent with the discussion of spin up in the hydrological cycle in *Dee et al.* [2011] and *Allan et al.* [2014].
7. Agreement of East African time series with observed rainfall features further corroborates the ability of the two-season method to correctly identify the seasons and confirms accurate rainfall representation, especially in the satellite-based data sets. The strong response to multiple El Niño events over the Horn of Africa further demonstrates the strength of this method in correctly capturing interannual variations in rainfall seasonality, and the wider scale responses (Figure 10) highlight further utility for meteorological analysis and some degree of potential predictability of this method.

This method proposed here has many advantages. Studies examining onset on a national scale often use an agricultural definition of the format "the first wet day of N consecutive days receiving at least P millimetres without a dry spell lasting n days and receiving less than p millimetres in the following C days" [*Boyard-Micheau et al.*, 2013]. However, as demonstrated by the differences in parameters used by *Mugalavai et al.* [2008] and *Ngetich et al.* [2014] when examining maize growth in Kenya, these are only locally applicable. In addition, data sets with different climatologies and rainfall amounts will give inconsistent onset and cessation dates or will require bias correcting. While such methods have value for community level decision support, they cannot be used continent wide to examine long-term changes in risk. However, the agreement between the method presented here and agriculturally motivated measures of seasonality suggests that this method could be used to assess agricultural risk continent wide. The low spatial density of weather stations means use of methods exploiting other meteorological variables, such as potential evapotranspiration (PET) [*Cook and Vizy*, 2012] or wind shear [*Omotosho*, 1992] are not suitable when examining observational data sets. In contrast, the method used here is universally applicable, as its single parameter is the local annual daily mean precipitation

which is defined uniquely for each grid point, thus accounting for regions with different rainfall totals and data sets with different rainfall biases.

Often, prior to the date when the wet season fully commences, heavy rainfall events can occur which are then followed by a prolonged dry period. This is termed a "false onset," as it appears that the wet season has begun. They present a large agricultural risk, as planting at the time of the false onset can lead to significant crop loss if the plants do not survive the intervening dry period [*Marteau et al.*, 2009; *Osorio and Galiano*, 2012]. Certain onset methods, such as methods based on thresholds of the cumulative percentage mean rainfall [*Odekunle*, 2006] or the method of *Cook and Vizy* [2012], comparing daily precipitation with PET, do not take into account such events. The method presented here takes into consideration false onsets, without the use of a fixed dry period (for example, 20–30 days [*Fitzpatrick et al.*, 2015]). A high rainfall event, followed by a prolonged dry period (characteristic of a false onset) would give a positive anomaly followed by a prolonged period of negative anomalies, resulting in the cumulative daily rainfall anomaly falling below its previous minima (before the large rainfall event). Thus, using the absolute minima as the onset removes the impact of false onsets.

There are some limitations, namely, the method requires consistent above average precipitation, giving a pronounced increase in the cumulative daily precipitation anomaly. Intermittent or light rainfall at the beginning and end of the wet season will be represented as a negative daily rainfall anomaly; therefore, these periods will not be considered as part of the wet season, potentially giving a reduced season length. Since onset/cessation can only be identified once the rainfall season is over, current applicability from an operational perspective is limited. However, the ability to highlight patterns in onset and cessation dates and their triggers will provide valuable information for forecast users. In addition, the method does not take into account locations that experience a major change in seasonal cycle from year to year. While the removal of regions with conflicting biannual/annual definitions should remove any impacts in these results, it should be taken into consideration for certain regions in future studies. Although all comparisons completed in this study, with both local onset methods and other papers, showed good agreement, comparison with other onset/cessation dates was not completed for all regions.

The results presented here raise important questions on the meaning of comparison metrics for data sets of African precipitation. Most studies comparing data sets of precipitation compare absolute amounts of rainfall [*Maidment et al.*, 2014; *Awange et al.*, 2016; *Novella and Thiaw*, 2013]. Here it has been demonstrated that data sets with contrasting rainfall quantities may exhibit good agreement in their representation of the seasonal cycle. The importance of the timing of the seasonal cycle in agricultural practice [*Oguntunde et al.*, 2014] means that good representation in data sets is crucial and suggests that a comparison of the seasonality of data sets should be included in intercomparison studies.

In conclusion, this paper has applied a consistent method of assessment of seasonality to six data sets of African precipitation. The results demonstrate strong agreement in the representation in the seasonal cycle in all the five satellite-based data sets, with moderate agreement in the reanalysis data set, and the robustness of the method of cumulative daily mean precipitation anomalies to determine the onset and cessation of the wet season(s) and capture the correct physical progression of the seasonal rains. This demonstrates that this method is suitable for use in further studies, including climate change analysis and model verification.

Acknowledgments

The authors would like to thank Rory Fitzpatrick and three anonymous reviewers for their reviews which lead to significant improvements of the paper. Caroline M. Dunning as supported with funding from a Natural Environment Research Council (NERC) PhD Studentship through the SCENARIO Doctoral Training Partnership grant NE/L002566/1. Emily C.L. Black was supported by the National Centre for Atmospheric Sciences climate division core research program. Richard P. Allan's contribution to the research leading to these results has received funding from the National Centre for Earth Observation and the European Union 7th Framework Programme (FP7/2007-2013) under grant agreement 603502 (EU project DACCIWA: Dynamics-aerosol-chemistry-cloud interactions in West Africa). All observational and reanalysis data sets exploited are publicly available data sets. ARCv2 data can be obtained from ftp://ftp.cpc.ncep.noaa.gov/fews/fewsdata/africa/arc2/bin/. The TARCATv2 data set is available from the TAMSAT website (http://www.met.reading.ac.uk/~tamsat/data). The CHIRPS data set, produced by the Climate Hazards Group, is available at http://chg.geog.ucsb.edu/data/chirps/#_Data. GPCP daily data are available from http://precip.gsfc.nasa.gov/. ERA-I data were sourced from the ECMWF using http://apps.ecmwf.int/datasets/data/interim-full-daily/{levtype}=sfc/. The TRMM 3B42 data were obtained from http://pmm.nasa.gov/data-access/downloads/trmm.

References

Adams, K. A., and E. K. Lawrence (2014), *Research Methods, Statistics, and Applications*, Sage Publ., Calif.

Adejuwon, J. O., and T. O. Odekunle (2006), Variability and the severity of the "little dry season" in southwestern Nigeria, *J. Clim.*, *19*(3), 483–493.

Allan, R. P., C. Liu, M. Zahn, D. A. Lavers, E. Koukouvagias, and A. Bodas-Salcedo (2014), Physically consistent responses of the global atmospheric hydrological cycle in models and observations, *Surv. Geophys.*, *35*, 533–552, doi:10.1007/s10712-012-9213-z.

Awange, J., et al. (2016), Uncertainties in remotely sensed precipitation data over Africa, *Int. J. Climatol.*, *36*(1), 303–323, doi:10.1002/joc.4346.

Balan Sarojini, B., P. A. Stott, E. Black, and D. Polson (2012), Fingerprints of changes in annual and seasonal precipitation from CMIP5 models over land and ocean, *Geophys. Res. Lett.*, *39*, L21706, doi:10.1029/2012GL053373.

Black, E., J. Slingo, and K. R. Sperber (2003), An observational study of the relationship between excessively strong short rains in coastal East Africa and Indian Ocean SST, *Mon. Weather Rev.*, *131*(1), 74–94.

Boyard-Micheau, J., P. Camberlin, N. Philippon, and V. Moron (2013), Regional-scale rainy season onset detection: A new approach based on multivariate analysis, *J. Clim.*, *26*(22), 8916–8928.

Camberlin, P., S. Janicot, and I. Poccard (2001), Seasonality and atmospheric dynamics of the teleconnection between African rainfall and tropical sea-surface temperature: Atlantic vs. ENSO, *Int. J. Climatol.*, *21*(8), 973–1005.

Camberlin, P., V. Moron, R. Okoola, N. Philippon, and W. Gitau (2009), Components of rainy seasons variability in equatorial East Africa: onset, cessation, rainfall frequency and intensity, *Theor. Appl. Climatol.*, *98*(3–4), 237–249.
Cook, K. H. (2001), A Southern Hemisphere wave response to ENSO with implications for southern Africa precipitation, *J. Atmos. Sci.*, *58*(15), 2146–2162.
Cook, K. H., and E. K. Vizy (2012), Impact of climate change on mid-twenty-first century growing seasons in Africa, *Clim. Dyn.*, *39*(12), 2937–2955.
Dee, D., et al. (2011), The ERA-Interim reanalysis: Configuration and performance of the data assimilation system, *Q. J. R. Meteorol. Soc.*, *137*(656), 553–597.
Diaconescu, E. P., P. Gachon, J. Scinocca, and R. Laprise (2015), Evaluation of daily precipitation statistics and monsoon onset/retreat over western Sahel in multiple data sets, *Clim. Dyn.*, *45*(5–6), 1325–1354.
Diem, J. E., S. J. Ryan, J. Hartter, and M. W. Palace (2014), Satellite-based rainfall data reveal a recent drying trend in central equatorial Africa, *Clim. Change*, *126*(1–2), 263–272.
Dong, B., and R. Sutton (2015), Dominant role of greenhouse-gas forcing in the recovery of Sahel rainfall, *Nat. Clim. Change*, *5*, 757–760.
Engelbrecht, C. J., W. A. Landman, F. A. Engelbrecht, and J. Malherbe (2015), A synoptic decomposition of rainfall over the Cape south coast of South Africa, *Clim. Dyn.*, *44*(9–10), 2589–2607.
Feng, X., A. Porporato, and I. Rodriguez-Iturbe (2013), Changes in rainfall seasonality in the tropics, *Nat. Clim. Change*, *3*(9), 811–815.
Fitzpatrick, R. G., C. L. Bain, P. Knippertz, J. H. Marsham, and D. J. Parker (2015), The West African monsoon onset: A concise comparison of definitions, *J. Clim.*, *28*(22), 8673–8694.
Funk, C., et al. (2015), The climate hazards infrared precipitation with stations—A new environmental record for monitoring extremes, *Scientific data*, *2*.
Hagos, S. M., and K. H. Cook (2007), Dynamics of the West African monsoon jump, *J. Clim.*, *20*(21), 5264–5284.
Hastenrath, S., D. Polzin, and C. Mutai (2007), Diagnosing the 2005 drought in equatorial East Africa, *J. Clim.*, *20*(18), 4628–4637.
Herrmann, S. M., and K. I. Mohr (2011), A continental-scale classification of rainfall seasonality regimes in Africa based on gridded precipitation and land surface temperature products, *J. Appl. Meteorol. Climatol.*, *50*(12), 2504–2513.
Hill, P. G., R. P. Allan, J. C. Chiu, and T. H. M. Stein (2016), A multisatellite climatology of clouds, radiation, and precipitation in southern West Africa and comparison to climate models, *J. Geophys. Res. Atmos.*, *121*, doi:10.1002/2016JD025246.
Hoell, A., and C. Funk (2014), Indo-Pacific sea surface temperature influences on failed consecutive rainy seasons over eastern Africa, *Clim. Dyn.*, *43*(5–6), 1645–1660, doi:10.1007/s00382-013-1991-6.
Huffman, G. J., R. F. Adler, M. M. Morrissey, D. T. Bolvin, S. Curtis, R. Joyce, B. McGavock, and J. Susskind (2001), Global precipitation at one-degree daily resolution from multisatellite observations, *J. Hydrometeorol.*, *2*(1), 36–50.
Huffman, G. J., D. T. Bolvin, E. J. Nelkin, D. B. Wolff, R. F. Adler, G. Gu, Y. Hong, K. P. Bowman, and E. F. Stocker (2007), The TRMM Multisatellite Precipitation Analysis (TMPA): Quasi-global, multiyear, combined-sensor precipitation estimates at fine scales, *J. Hydrometeorol.*, *8*(1), 38–55.
Issa Lélé, M., and P. J. Lamb (2010), Variability of the Intertropical Front (ITF) and rainfall over the West African Sudan-Sahel zone, *J. Clim.*, *23*(14), 3984–4004.
Kenya Food Security Steering Group (KFSSG) (2010), *The 2010 Long Rains Season Assessment Report*. [Available at http://www.fao.org/fileadmin/user_upload/drought/docs/Kenya_2010_LRA%20Report.pdf.]
Kniveton, D. R., R. Layberry, C. J. R. Williams, and M. Peck (2009), Trends in the start of the wet season over Africa, *Int. J. Climatol.*, *29*(9), 1216–1225.
Kyte, E. A., G. D. Quartly, M. A. Srokosz, and M. N. Tsimplis (2006), Interannual variations in precipitation: The effect of the North Atlantic and Southern Oscillations as seen in a satellite precipitation data set and in models, *J. Geophys. Res.*, *111*, D24113, doi:10.1029/2006JD007138.
Liebmann, B., and J. Marengo (2001), Interannual variability of the rainy season and rainfall in the Brazilian Amazon Basin, *J. Clim.*, *14*(22), 4308–4318.
Liebmann, B., I. Bladé, G. N. Kiladis, L. M. Carvalho, G. B. Senay, D. Allured, S. Leroux, and C. Funk (2012), Seasonality of African precipitation from 1996 to 2009, *J. Clim.*, *25*(12), 4304–4322.
Lott, F. C., N. Christidis, and P. A. Stott (2013), Can the 2011 East African drought be attributed to human-induced climate change?, *Geophys. Res. Lett.*, *40*(6), 1177–1181, doi:10.1002/grl.50235.
Lyon, B., and D. G. DeWitt (2012), A recent and abrupt decline in the East African long rains, *Geophys. Res. Lett.*, *39*(2), L02702, doi:10.1029/2011GL050337.
Maidment, R. I., D. Grimes, R. P. Allan, E. Tarnavsky, M. Stringer, T. Hewison, R. Roebeling, and E. Black (2014), The 30 year TAMSAT African Rainfall Climatology And Time series (TARCAT) data set, *J. Geophys. Res. Atmos.*, *119*(18), 10–619.
Maidment, R. I., R. P. Allan, and E. Black (2015), Recent observed and simulated changes in precipitation over Africa, *Geophys. Res. Lett.*, *42*(19), 8155–8164, doi:10.1002/2015GL065765.
Marteau, R., V. Moron, and N. Philippon (2009), Spatial coherence of monsoon onset over western and central Sahel (1950–2000), *J. Clim.*, *22*(5), 1313–1324.
Mounkaila, M. S., B. J. Abiodun, and J. Omotosho (2015), Assessing the capability of CORDEX models in simulating onset of rainfall in West Africa, *Theor. Appl. Climatol.*, *119*(1–2), 255–272.
Mugalavai, E. M., E. C. Kipkorir, D. Raes, and M. S. Rao (2008), Analysis of rainfall onset, cessation and length of growing season for western Kenya, *Agric. For. Meteorol.*, *148*(6), 1123–1135.
Ngetich, K., M. Mucheru-Muna, J. Mugwe, C. Shisanya, J. Diels, and D. Mugendi (2014), Length of growing season, rainfall temporal distribution, onset and cessation dates in the Kenyan highlands, *Agric. For. Meteorol.*, *188*, 24–32.
Nguyen, H., C. D. Thorncroft, and C. Zhang (2011), Guinean coastal rainfall of the West African Monsoon, *Q. J. R. Meteorol. Soc.*, *137*(660), 1828–1840.
Nicholson, S. E. (2000), The nature of rainfall variability over Africa on time scales of decades to millenia, *Global Planet. Change*, *26*(1), 137–158.
Nicholson, S. E. (2013), The West African Sahel: A review of recent studies on the rainfall regime and its interannual variability, *ISRN Meteorol.*, *2013*, 1–32.
Nikulin, G., et al. (2012), Precipitation climatology in an ensemble of CORDEX-Africa regional climate simulations, *J. Clim.*, *25*(18), 6057–6078.
Novella, N. S., and W. M. Thiaw (2013), African rainfall climatology version 2 for famine early warning systems, *J. Appl. Meteorol. Climatol.*, *52*(3), 588–606.

Odekunle, T. (2006), Determining rainy season onset and retreat over Nigeria from precipitation amount and number of rainy days, *Theor. Appl. Climatol.*, *83*(1–4), 193–201.
Oguntunde, P. G., G. Lischeid, B. J. Abiodun, and O. Dietrich (2014), Analysis of spatial and temporal patterns in onset, cessation and length of growing season in Nigeria, *Agric. For. Meteorol.*, *194*, 77–87.
Okoloye, C., N. Aisiokuebo, J. Ukeje, A. Anuforom, and I. Nnodu (2014), Rainfall variability and the recent climate extremes in Nigeria, *J. Meteorol. Clim. Sci.*, *11*(1), 49–57.
Omotosho, J. (1992), Long-range prediction of the onset and end of the rainy season in the West African Sahel, *Int. J. Climatol.*, *12*(4), 369–382.
Osorio, J. G., and S. G. Galiano (2012), Non-stationary analysis of dry spells in monsoon season of Senegal River Basin using data from regional climate models (RCMs), *J. Hydrol.*, *450*, 82–92.
Paeth, H., et al. (2011), Progress in regional downscaling of West African precipitation, *Atmos. Sci. Lett.*, *12*(1), 75–82.
Philippon, N., P. Camberlin, V. Moron, and J. Boyard-Micheau (2015), Anomalously wet and dry rainy seasons in equatorial East Africa and associated differences in intra-seasonal characteristics, *Clim. Dyn.*, *45*(7), 2101–2121.
Rao, K., W. Ndegwa, K. Kizito, and A. Oyoo (2011), Climate variability and change: Farmer perceptions and understanding of intra-seasonal variability in rainfall and associated risk in semi-arid Kenya, *Exp. Agric.*, *47*(2), 267–291.
Sanogo, S., A. H. Fink, J. A. Omotosho, A. Ba, R. Redl, and V. Ermert (2015), Spatio-temporal characteristics of the recent rainfall recovery in West Africa, *Int. J. Climatol.*, *35*(15), 4589–4605, doi:10.1002/joc.4309.
Shongwe, M. E., C. Lennard, B. Liebmann, E.-A. Kalognomou, L. Ntsangwane, and I. Pinto (2015), An evaluation of CORDEX regional climate models in simulating precipitation over southern Africa, *Atmos. Sci. Lett.*, *16*(3), 199–207.
Sultan, B., and S. Janicot (2003), The West African monsoon dynamics. Part II: The "preonset" and "onset" of the summer monsoon, *J. Clim.*, *16*(21), 3407–3427.
Sylla, M. B., E. Coppola, L. Mariotti, F. Giorgi, P. Ruti, A. Dell'Aquila, and X. Bi (2010), Multiyear simulation of the African climate using a regional climate model (RegCM3) with the high resolution ERA-interim reanalysis, *Clim. Dyn.*, *35*(1), 231–247.
Tadross, M., B. Hewitson, and M. Usman (2005), The interannual variability of the onset of the maize growing season over South Africa and Zimbabwe, *J. Clim.*, *18*(16), 3356–3372.
Tarnavsky, E., D. Grimes, R. Maidment, E. Black, R. P. Allan, M. Stringer, R. Chadwick, and F. Kayitakire (2014), Extension of the TAMSAT satellite-based rainfall monitoring over Africa and from 1983 to present, *J. Appl. Meteorol. Climatol.*, *53*(12), 2805–2822.
Thorncroft, C. D., H. Nguyen, C. Zhang, and P. Peyrillé (2011), Annual cycle of the West African monsoon: Regional circulations and associated water vapour transport, *Q. J. R. Meteorol. Soc.*, *137*(654), 129–147.
USAID FEWS NET (2004), *Kenya Food Security Report—July 7*. [Available at http://www.fews.net/sites/default/files/documents/reports/Kenya_200407en.pdf.]
Van de Giesen, N., J. Liebe, and G. Jung (2010), Adapting to climate change in the Volta Basin, West Africa, *Curr. Sci.*, *98*(8), 1033–1037.
Washington, R., R. James, H. Pearce, W. M. Pokam, and W. Moufouma-Okia (2013), Congo Basin rainfall climatology: Can we believe the climate models?, *Philos. Trans. R. Soc. London, Ser. B*, *368*(1625), 20120296.
Weldon, D., and C. Reason (2014), Variability of rainfall characteristics over the South Coast region of South Africa, *Theor. Appl. Climatol.*, *115*(1–2), 177–185.
Wilks, D. S. (2011), *Statistical Methods in the Atmospheric Sciences*, vol. 100, Academic Press, Waltham, Mass.
Yamada, T. J., S. Kanae, T. Oki, and R. D. Koster (2013), Seasonal variation of land-atmosphere coupling strength over the West African monsoon region in an atmospheric general circulation model, *Hydrol. Sci. J.*, *58*(6), 1276–1286.
Yang, G.-Y., and J. Slingo (2001), The diurnal cycle in the tropics, *Mon. Weather Rev.*, *129*(4), 784–801.
Yang, W., R. Seager, M. A. Cane, and B. Lyon (2014), The East African long rains in observations and models, *J. Clim.*, *27*(19), 7185–7202.
Yang, W., R. Seager, M. A. Cane, and B. Lyon (2015a), The rainfall annual cycle bias over East Africa in CMIP5 coupled climate models, *J. Clim.*, *28*(24), 9789–9802.
Yang, W., R. Seager, M. A. Cane, and B. Lyon (2015b), The Annual Cycle of East African Precipitation, *J. Clim.*, *28*(6), 2385–2404.
Young, M. P., C. J. Williams, J. C. Chiu, R. I. Maidment, and S.-H. Chen (2014), Investigation of discrepancies in satellite rainfall estimates over Ethiopia, *J. Hydrometeorol.*, *15*(6), 2347–2369.
Zhang, G., and K. H. Cook (2014), West African monsoon demise: Climatology, interannual variations, and relationship to seasonal rainfall, *J. Geophys. Res. Atmos.*, *119*(17), 10,175–10,193, doi:10.1002/2014JD022043.